Supporting Information for "Modeling the Effects of Topography Heterogeneity and Discharge Variations on Riverbed Hydrodynamics in a 30-kilometer-long Reach over a Nine-year Period using OpenFOAM"

Yunxiang Chen[1], Jie Bao[1], Yilin Fang[1], Timothy Scheibe[1], Marshall Richmond[1], William Perkins[1], Huiying Ren[1], , Xuehang Song[1], Zhuoran Duan[1], Zhangshuan Hou[1], Xiaoliang He[1]

[1]Pacific Northwest National Laboratory, Richland, WA, USA

Contents of this file

1. Text S1 to S2.
2. Figure S1 to S12.
3. Table S1 to S2.

Introduction

This file contains two supplementary texts, ten supplementary figures, and two tables. Text S1 analyzes 11 potential uncertainty in our model and shows that these errors can be well managed using the approaches proposed in our paper. Text S2 describes how to decompose a streambed into multiple patches and how these patches are converted to the recognizable boundary patches in OpenFOAM. Figure S1 to Figure S12 show the supplementary figures for the main text and for supporting the uncertainty analyses.

Table 1 and Table 2 show the coordinates of the survey locations and model constants of the $k-\omega$ SST model.

Text S1: uncertainty analyses

Computation fluid dynamics (CFD) modeling of streamflow in large-scale rivers over long time periods involves uncertainties from observations, fluid dynamics theories, and numerical techniques. We quantify and analyze 11 sources of uncertainties from (1) water surface elevation (WSE) observation, (2) riverbed bathymetry measurement, (3) rough wall resistance model, (4) roughness calibration using WSE, (5) free surface definition from the volume of fluid, (6) representing streambed using zig-zag grid, (7) mesh resolution, (8) time step, (9) linearization of velocity-velocity and velocity-pressure coupling, (10) discretization schemes, and (11) interpolation between the CFD mesh and a uniform mesh in postprocessing.

As the calibrated roughness parameter is a crucial parameter in our model, the uncertainty in WSE observation may affect the accuracy of calibration and CFD modeling. In particular, this work identifies the locally optimal roughness parameter as the value makes the mean error (ME) between the modeled WSE and the observed ones to be zero (see Section 2.4). This means that the time-averaged value of WSE from observation determines the calibration accuracy. To illustrate the uncertainty in WSE observations, Figure S5 shows a comparison of the WSE at 100B observed at two nearby locations. The results show that the ME between observation 2 and observation 1 is 3.219 cm, however, the standard deviation between the two observations is 11.555 cm (Figure S5b). We argue that the large standard deviation is attributed to a small time uncertainty during the observation. This can be proved by Figure S5c which shows that the standard deviation

reduces to 4.763 cm if the time history in observation 2 is shifted by 39.3 minutes. However, Figure S5c also means the time shift does not contribute to a large uncertainty in its mean value as the ME is always in the range 3.08 cm $\sim$ 3.22 cm for any time shift between -120 minutes and 120 minutes. As the mean value of WSE is used to calibrate roughness, the above results thus demonstrate that the current WSE survey technique does not bring significant uncertainty for roughness quantification but could result in a large difference in standard deviation, mean absolute error, and root mean square when comparing the modeled WSE to observed ones. Actually, if we do an alignment of observation 2, i.e., shifting observation 2 by 39.3 minutes in time and adding 3.2 cm to its value, we see that the difference between observation 1 and such an aligned WSE is clearly reduced (Figure S5b).

Natural streambeds usually have diverse scales that affect the fluid dynamics and biogeochemistry. It is difficult to measure all of these scales; however, it is necessary to have a brief discussion of these scales and the effect of river topography measurements on CFD modeling. In this work, the LiDAR measured riverbed has a vertical resolution of 1 m, which means all topographic features that are less 1 m are not represented in the streambed bathymetry. These scales can be further divided into fine scale (7.8 μm $\sim$ 2 mm) and coarse-grain scale (2 mm $\sim$ 0.256 m) (Berenbrock & Tranmer, 2008). The fine scale sediments, e.g., slit, clay, and sand, are usually suspended in water due to small-scale turbulence (Ongley, 1996) and the coarse-grain scale sediments, e.g., gravels, cobbles, and boulders (Ongley, 1996), control the flow separation, sweep and ejection events, and formation of large coherent structures (Hardy et al., 2010). In this work, the effect of these scales on the streamflow is considered by adjusting the streambed roughness to enable

a match between the modeled WSE and the observed ones (see calibration accuracy in Section 3.1 and more discussion in Section 4.1).

It is important to note that the roughness calibration using the observed WSE depends on two fluid dynamics assumptions. Firstly, it assumes that the WSE monotonically increases with increasing streambed flow resistance; and secondly, it assumes that the roughness wall resistance model used in this work is valid for quantifying streambed resistance for natural rivers. The former has been demonstrated as in Figure 3a and Figure S1. The latter can be indirectly proved by another study that predicts 96% of the theoretical flow resistance using the same rough wall resistance approach (see case S3b in (Chen et al., 2018)). Despite these justifications, the high calibration accuracy (Section 3.1) and the prediction accuracy over short, medium, and long time periods (Section 3.2 $\sim$ Section 3.4) further demonstrate the effectiveness of the two assumptions adopted here.

As the volume of fluid is used to calculate the free surface, a volume fraction of 0.5 may bring uncertainty to the definition of the modeled WSE. Though choosing 0.5 to define a free surface is a common practice (Hirt & Nichols, 1981), we argue that the potential uncertainty due to such a definition can be well managed during the roughness calibration procedure because any changes in WSE due to free surface definition are incorporated into the calibrated roughness parameter when modeled WSE agrees with the observed ones. Regarding the uncertainty of representing the streambed using a zig-zag grid, it has been discussed in Section 2.3 and it is shown that such uncertainty is automatically considered during the roughness calibration.

The mesh resolution and time step are common sources of uncertainty of CFD models. As one goal of this paper is to predict the total pressure at the streambed, a summation

of the hydrodynamic pressure and the hydrostatic pressure, for subsurface models, Figure S11 shows the difference and the 1:1 plot of the total pressure head between a fine mesh (20 m $\times$ 20 m $\times$ 0.5 m) and a coarse mesh (20 m $\times$ 20 m $\times$ 1 m) at the time 16PM Jan-16-2013. The result shows that the difference is in the range -0.1 m $\sim$ 0.1 m at most of the locations and the spatial average difference is -0.03 m (Figure S11a). The 1:1 plot also shows that the total pressure head from the two meshes almost overlaps with a mean difference, a root mean square, and a R^2 value as -0.03 m, 0.1 m, and 0.9987, respectively. Recalling that the WSE (related to the hydrostatic pressure head) observation itself could have an uncertainty of 0.032 m (Figure S5c) and the average value of dynamic pressure head is -0.353 m (Figure 13c), the uncertainty attributed to mesh resolution is either of the similar order water stage observation or 8.5% of the average dynamic pressure. This suggests that the mesh resolution does not contribute significant error to the total pressure head. To further evaluate the effect of time step, Figure S4 shows a comparison of the modeled WSE using five different time steps at the six observation locations. The results reveal that the time step tested here does not affect the accuracy of WSE. Therefore, we choose the time step 3 s for the prediction simulations in order to reduce computational costs (see Section 2.7).

Regarding the uncertainty from the linearization of velocity-velocity and velocity-pressure coupling (Equation 2), it has been proved that using the Pressure Implicit with Splitting of Operators (PISO) algorithm (Issa, 1985) does not bring big errors to CFD modeling results (see details of PISO implementation in OpenFOAM and uncertainty analyses in Chen et al. (2018)). For the discretization schemes, Figure S4 shows that the time step does not affect WSE, which suggests the temporal discretization scheme has

little influence on the modeling accuracy. For the spatial derivatives, use of the second-order schemes for advection and diffusion terms means they do not contribute significant errors (see uncertainty analyses in Chen et al. (2018)).

The final uncertainty is related to interpolating the CFD results, e.g., WSE, total pressure, dynamic pressure, bed shear stress, from the OpenFOAM mesh to a uniform mesh for postprocessing. Figure S12 compares the bed shear stress interpolated based on a self-developed Matlab code and that interpolated from ParaView (www.paraview.org), an open-source, multiplatform data analysis and visualization software. The result shows that the Matlab code has similar accuracy as ParaView. For easier comparison, the Matlab code is available at Velo (sbrsfa.velo.pnnl.gov).

Overall, the above analyses identify potential sources in our modeling approach and highlight the importance of accurate measurements of water stage while other uncertainties are either not important or can be reduced through the calibration procedure.

Text S2: surface decomposition

The surface decomposition is used to generate a distributed roughness for OpenFOAM, which is implemented as follows: (a) calculating a centerline of the river bed (blue line in Figure 3c); (b) drawing a straight line passing through each observation location (red dots) and perpendicular to the centerline; (c) calculating the intersected point (blue squares) between each straight line and the centerline; (d) generating a dividing point (stars) between two neighbouring intersected points along the centerline; (e) adding two boundary points (stars at inlet and outlet) as dividing points and generating straight lines perpendicular to the centerline and decomposing the river bed into 8 pieces; (f) extending each piece in river depth direction (z) to form 8 close STL surfaces; (g) reading OpenFOAM

mesh and grouping faces on river bed into 8 groups by checking if a face belongs to an STL surface; (h) assigning calibrated k_s at 100B for region 0 and 1, assigning calibrated k_s at 100N, 100D, LI, and 100H for region 2-5, and assigning calibrated k_s at 100F for region 6 and 7; and (i) writing the new boundary and k_s value into OpenFOAM mesh. Here the domain number 8 is used as an example and it could also be 1, 2, and 50 as shown in Table 1 and Figure S3b. To facilitate future applications, the Matlab code relevant to the above procedures is shared in Velo (sbrsfa.velo.pnnl.gov).

References

Berenbrock, C., & Tranmer, A. W. (2008). Simulation of flow, sediment transport, and sediment mobility of the Lower Coeur d'Alene River, Idaho. *USGS Scientific Investigations Report*(2008-5093), 164.

Chen, Y., DiBiase, R. A., McCarroll, N., & Liu, X. (2019). Quantifying flow resistance in mountain streams using computational fluid dynamics modeling over structure-from-motion photogrammetry-derived microtopography. *Earth Surface Processes and Landforms*, *44*(10), 1973–1987. doi: 10.1002/esp.4624

Chen, Y., Liu, X., Gulley, J. D., & Mankoff, K. D. (2018). Subglacial conduit roughness: insights from computational fluid dynamics models. *Geophysical Research Letters*, *45*(20), 11206–11218. doi: 10.1029/2018GL079590

Hardy, R. J., Best, J. L., Lane, S. N., & Carbonneau, P. E. (2010). Coherent flow structures in a depth-limited flow over a gravel surface: The influence of surface roughness. *Journal of Geophysical Research*, *115*(F3), F03006. doi: 10.1029/2009JF001416

Hirt, C., & Nichols, B. (1981). Volume of fluid (VOF) method for the dynamics of free boundaries. *Journal of Computational Physics*, *39*(1), 201–225. doi: 10.1016/

0021-9991(81)90145-5

Issa, R. I. (1985). Solution of the implicitly discretised fluid flow equations by operator-splitting. *Journal of Computational Physics*, *62*, 40–65. doi: 10.1016/0021-9991(86)90099-9

Jeong, J., & Hussain, F. (1995). On the identification of a vortex. *Journal of Fluid Mechanics*, *285*, 69–94. doi: 10.1017/S0022112095000462

Ongley, E. (1996). Ch13: Sediment measurements. In B. Jamie & B. Richard (Eds.), *Water quality monitoring : a practical guide to the design and implementation of freshwater quality studies and monitoring programs* (1st ed., p. 400). London, U.K.: E & FN SPON.

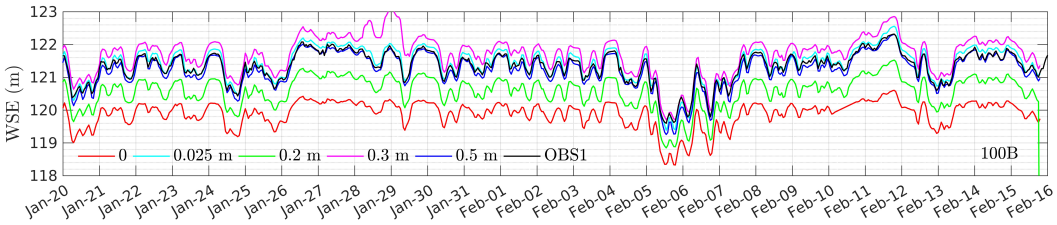

Figure S1. A comparison between observed WSE at 100B and modeled ones using different roughness height.

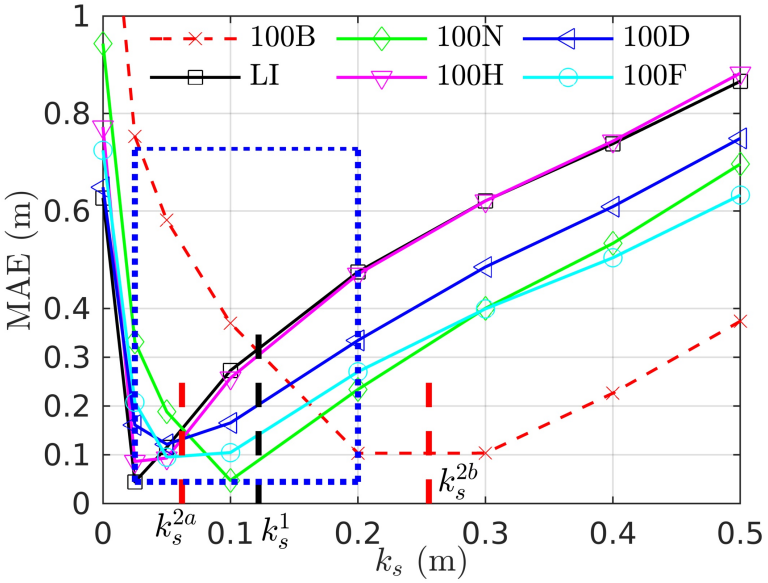

Figure S2. The variation of mean absolute error (MAE) between modeled and observed WSE at six locations using different roughness parameters. Black and red vertical lines represent the optimal roughness height using one-ks and two-ks strategy.

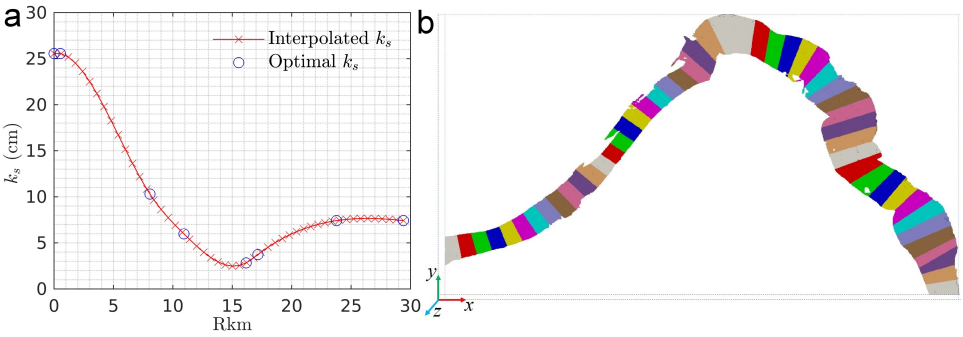

Figure S3. The roughness height on 50 pieces of stream interpolated from the 6 globally optimal roughness parameter (blue circle) (a) and the decomposition of the streambed into 50 pieces (b).

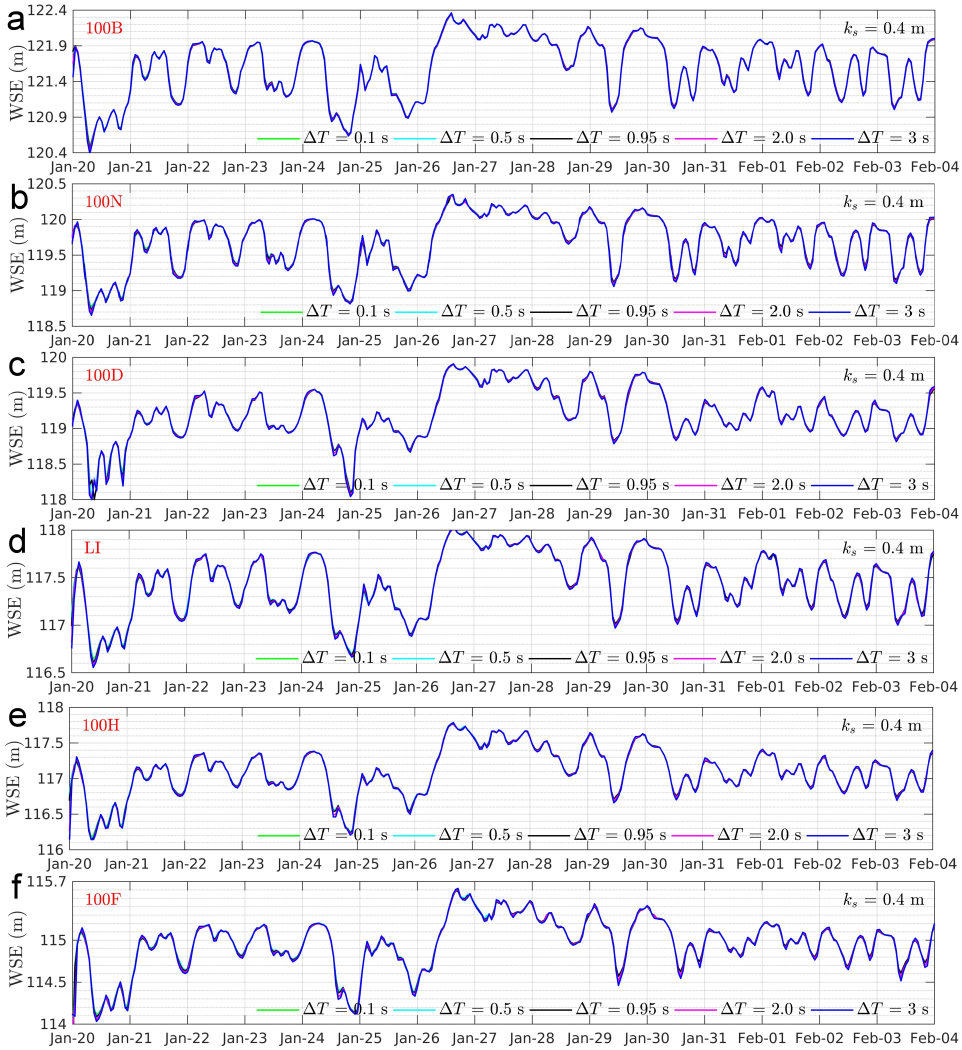

Figure S4. A comparison of WSE at different time step at 100B, 100N, 100D, LI, 100H, and 100F.

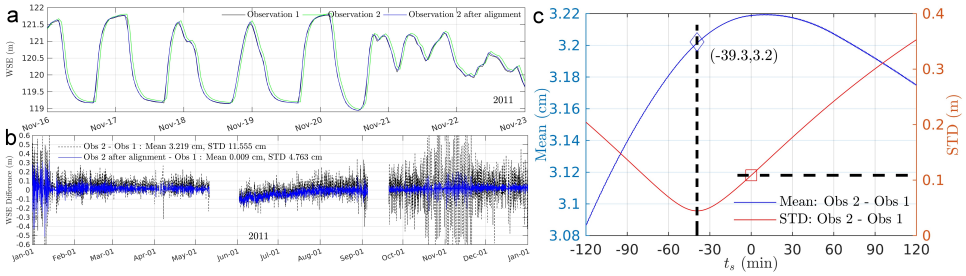

Figure S5. A comparison of WSE at 100B from observation 1, observation 2, and observation 2 after alignment (a), the differences in WSE between observation 1 and observation 2 and that between observation 1 and observation 2 after alignment (b), and the mean and standard deviation between observation 1 and observation 2 with a time shift t_s (c).

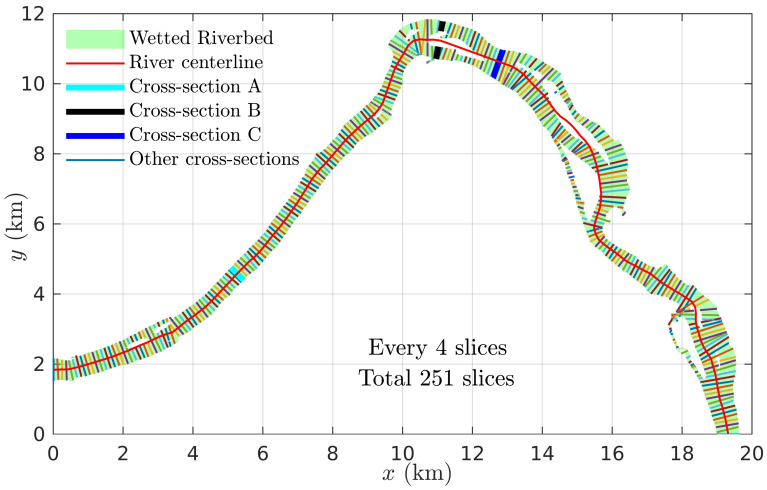

Figure S6. A sketch showing how to generate cross-sections perpendicular to the river centerline.

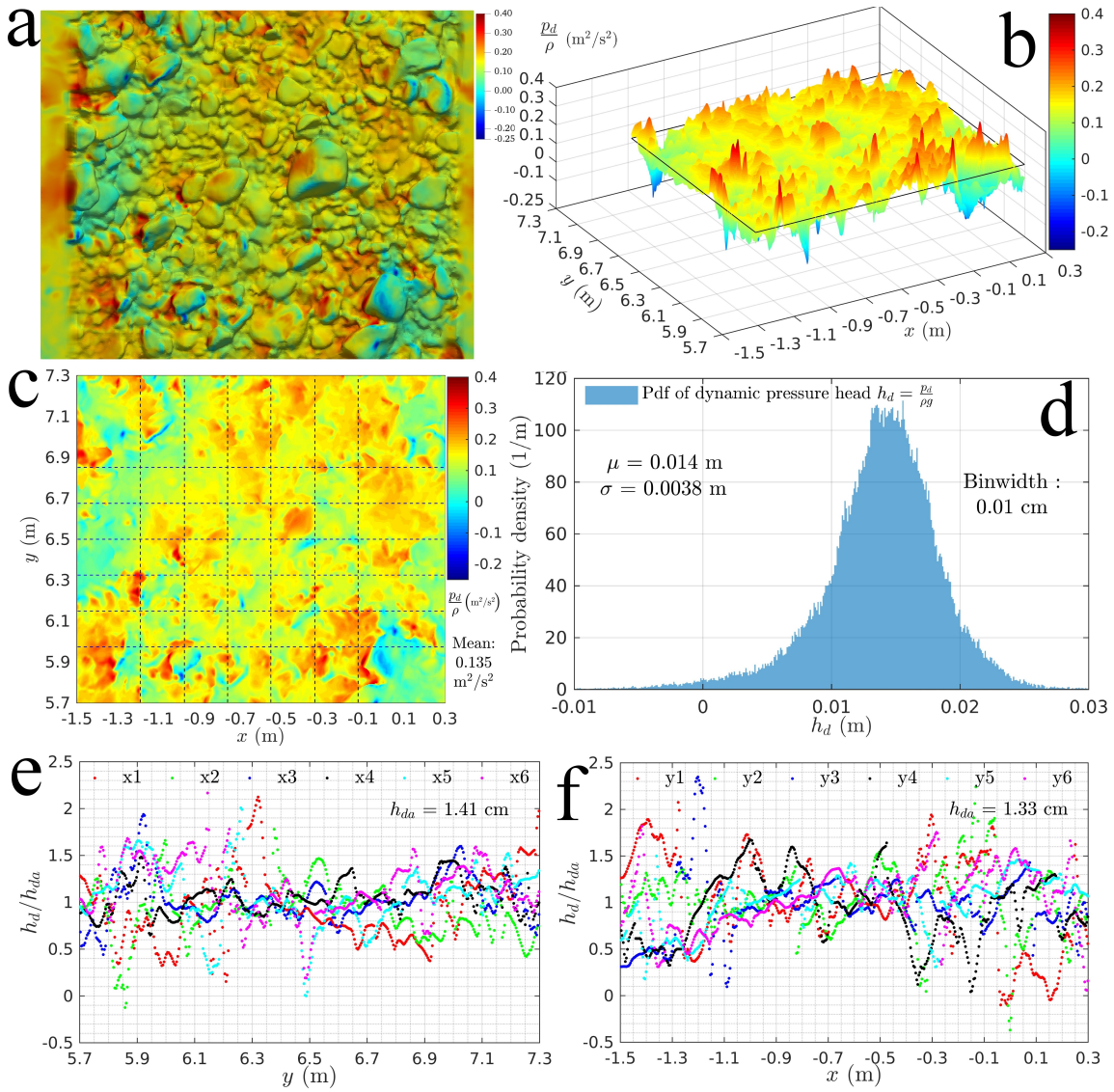

Figure S7. The distribution of dynamic pressure on a mm scale resolution riverbed in Pennsylvania. (a) Dynamic pressure plotted on the streambed; (b) 3D view of the dynamic pressure distribution; (c) top view of the dynamic pressure distribution; (d) probability density function of the dynamic pressure on the bed; (e-f), variations of normalized dynamic pressure head along the spanwise (y) and streamwise (x) direction. Horizontal and vertical lines on (c) denote locations y1-y6 (bottom to top) and x1-x6 (left to right) respectively. The water depth, flow velocity, standard deviation of the streambed and the median particle size is 0.168 m, 0.5 m/s, 0.028 m, and 0.06 m, respectively. More details of the data can be found as the case BC1 in Chen et al. (2019).

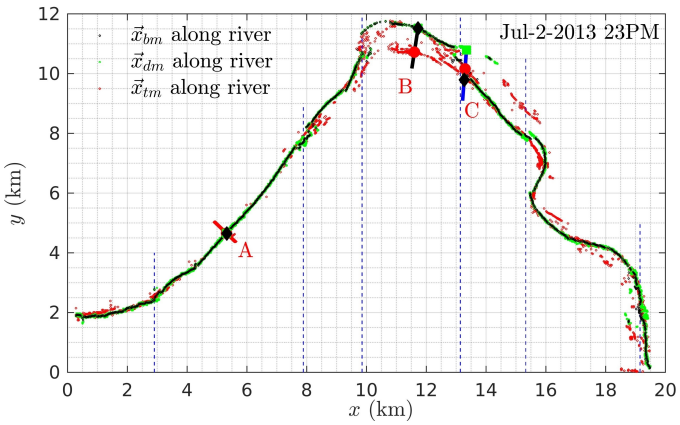

Figure S8. The locations of bathymetry minimum, water depth maximum, and shear stress maximum along the river centerline at 23PM Jul-2-2013.

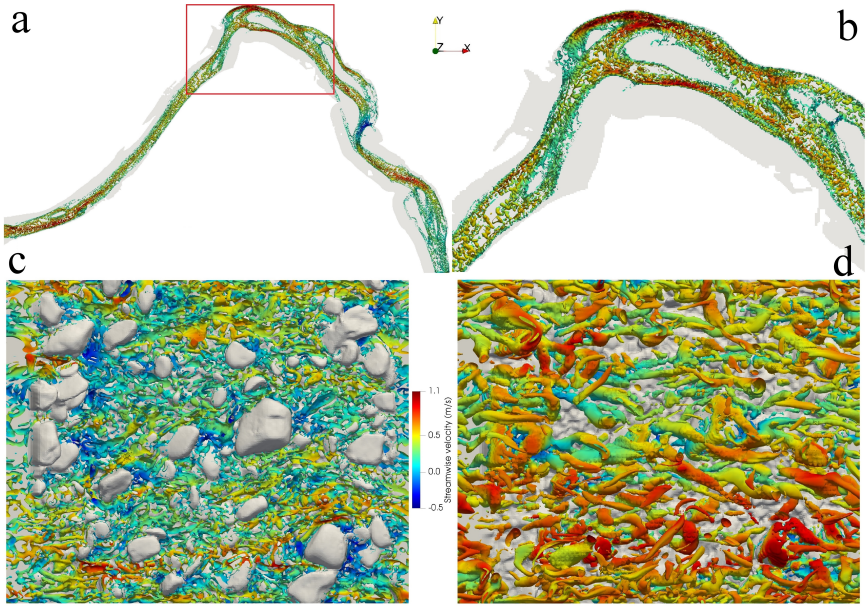

Figure S9. The vortex structure in the Columbia River (a,b) and near a streambed in Pennsylvania (c,d). (b) is the zoom in of the red box in (a). The lowest and highest points on the streambed are 0.01 and 0.19 m. (c,d) show vortex structure below and above 0.1 m. The vortex structure is quantified by λ_2 (Jeong & Hussain, 1995). More details of the data can be found as the case BC1 in Chen et al. (2019).

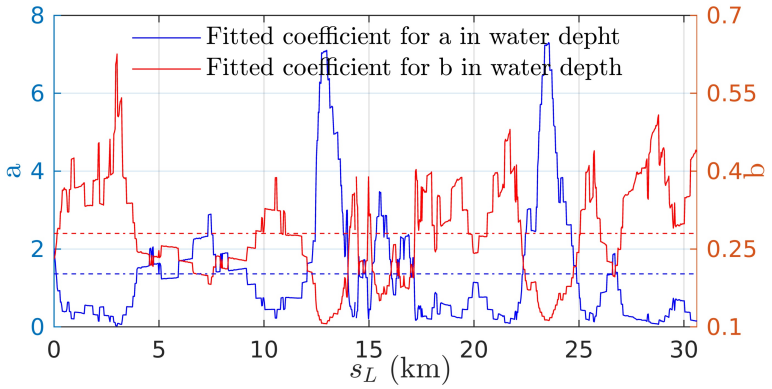

Figure S10. Variations of the fitting parameters for water depth along the streamwise coordinate.

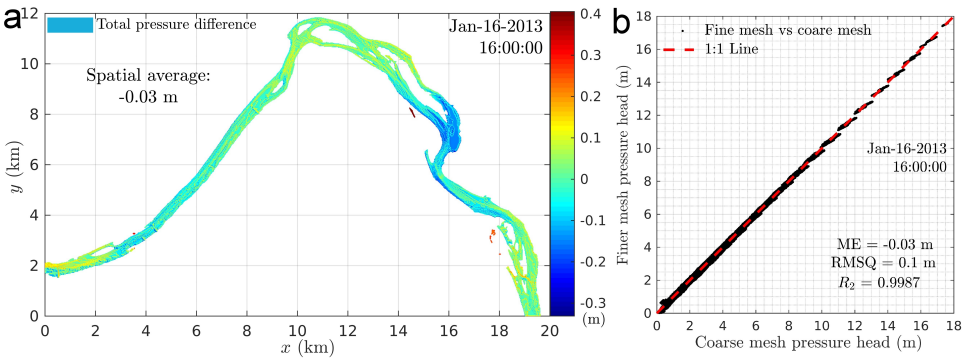

Figure S11. Distribution of the difference between total pressure modeled with a fine mesh and a coarse mesh (a), and the 1:1 plot of the total pressure from the fine mesh and the coarse mesh (b).

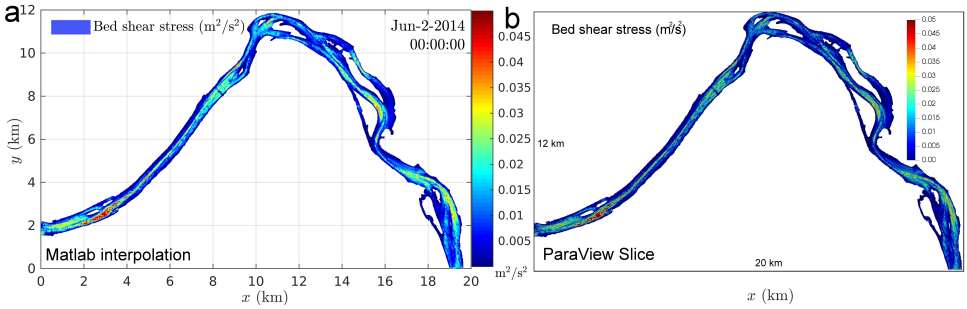

Figure S12. A comparison of the bed shear stress interpolated by Matlab code (a) and ParaView (b).

Table S1. Horizontal coordinates and bed elevation of survey locations.

Station	x (m)	y (m)	z_b (m)
100B	555.63	1619.60	117.69
100N	6759.03	5882.76	116.26
100D	8516.19	8082.07	119.05
LI	12580.24	10298.23	113.74
100H	13260.85	9756.13	114.45
100F	16676.44	4429.60	110.77
100HD	15451.55	7581.22	112.61

Table S2. Coefficients of $k-\omega$ turbulence model

β^*	$\alpha_{\omega 1}$	$\alpha_{\omega 2}$	α_{k1}	α_{k2}	β_1	β_2	γ_1	γ_1	a_1	b_1	c_1	C_μ
0.09	0.5	0.856	0.85	1	0.075	0.0828	0.555556	0.44	0.31	1	10	0.09